

Parametric Analysis of the Optical Behavior of a Linear Fresnel Reflector

Elmaanaoui Youssef *, Saifaoui Dennoun

Department of Physics, University of Hassan II, Casablanca, Morocco

ABSTRACT

This study presents a parametric analysis of the optical efficiency of a Linear Fresnel Reflector (LFR) using a Monte Carlo Ray Tracing tool. Parameters considered in this analysis are the design profile angle (DPA), the total solar field width, the total solar field length, the location's latitude (ϕ), day of the year, and time of the day. Besides, a case study is presented comparing five different cities using the annual mean and monthly mean heat transferred to the outer surface of the absorber tube and operational hours. Results related to the optical analysis show that the best locations to operate an LFR are at low latitudes ($\phi < 20^\circ$) using a high DPA in the modeling process of the solar field. However, the case study showed that the available DNI resources play a significant role in determining how much a given LFR will make use of its high optical efficiency. In fact, it was found that cities with lower annual optical efficiencies and operational hours had better annual mean heat transferred to the outer surface of the absorber tube due to the high DNI resources of the location.

Keywords: Linear Fresnel Reflector; optical efficiency; Ray tracing; Incident Angle Modifier; Case study.

I. INTRODUCTION

A linear Fresnel reflector (LFR) is a line focusing Concentrated Solar Power technology (CSP) [1]–[4]. It uses flat or slightly bent reflecting mirrors that track the sun on one axis to reflect incoming sunlight into a receiver mounted few meters above these reflecting mirrors [5]–[7]. Even though LFR is regarded to as a promising technology that can reduce the Levelized Cost Of Electricity (LOCE) [8], [9], it suffers from low optical efficiency compared to other CSP technologies [3], [5], [8]. This low optical efficiency is attributed to some optical effects present in the solar field, which are shading, blocking, end loss, and cosine effect [10], [11].

Shading occurs when a reflecting mirror finds itself under the shadow of the neighboring one, thus a portion of this mirror becomes useless [5], [12]. In other words, when shading occurs, the real reflecting area of the LFR solar field diminishes [13]. Another source of shading is wide receivers or secondary concentrators [14]. In a north-south solar field, shading only occurs early in the

morning and late in the afternoon when the sun is low in the sky [15], and it is more important in high latitude locations [16].

Blocking appears when reflected sunrays are intercepted by a neighboring mirror instead of being collected at the receiver [5], [12]. Once more, when such effect occurs, the useful area of the solar field diminishes [13]. Contrary to shading, blocking only appears in the middle of the day when the sun is high in the sky [17], and it is less important than shading [13]. Both blocking and shading effects are only related to the transversal plane and vary with the variation of the transversal incidence angle.

In a north-south LFR solar field, end loss takes place in the longitudinal plane and gives an idea about the portion of the receiver that is not illuminated by the reflected sunrays [18]. End loss occurs especially at low longitudinal incidence angle and it is more important at high latitude locations [19], [20]. However, for very long receivers, end loss can be neglected [19], [20].

Cosine effect describes the reduction of solar energy due to the reflecting mirrors not being normal to the incoming sunrays [18]. Unlike the previous effects that are only related to either the transversal or the longitudinal planes, the cosine effect occurs in both planes [5], [18]. Losses due to cosine effect are more important in the morning and the afternoon and increase at high latitude locations [2], [19], [20].

The aforementioned optical effects, especially shading and blocking, have been subject to several works that analyzed them in an attempt to understand the overall optical behavior of the LFR solar field [10], [15], [16], [21], [22]. Meanwhile, the optical efficiency itself is calculate otherwise, generally, using a Monte Carlo Ray Tracing tool (whether it is an in-house developed code or a commercial software). In a ray tracing technique, several rays are applied on the solar field and data about the reflected rays that reach the receiver are collected. Using these data, the optical efficiency of the LFR can be estimated without any need to go deep in analyzing all the optical effects present within the solar field. Nevertheless, an effective interpretation of the ray tracing results requires a good understanding of the impact of each optical effect on the LFR performances since the optical efficiency is nothing more than the combination of all previously mentioned effects.

The optical efficiency of the LFR system has been subject to several published papers, most of it relied on ray tracing technique. Some authors presented in their works solutions to overcome the different optical losses present in the LFR solar field in an attempt to enhance its overall optical efficiency. These works can be categorized into two different families. In the first family, we found works that interested in varying different LFR components to get to better optical efficiency without modifying the LFR concept itself [9], [12], [23]. While in the second family, we found works that completely modified the LFR concept proposing novel ones such as the compact LFR [24], the etendue-matched LFR [25], and the elevation LFR [26].

The present study can be categorized within the first family of works since it deals with a standard LFR presenting a parametric analysis of its optical efficiency. The parameters taken into consideration in this work are the design profile angle (DPA), the total solar field width, the total solar field length, the location where the LFR is installed, days of the year, and time of the day. The analysis is performed using a well-known Monte

Carlo Ray Tracing software commonly encountered in such studies and a special attention was given to the Incident Angle Modifier (IAM). In the second part of this work, a case study is presented where five different cities are compared using the annual mean heat transferred, monthly mean heat transferred, and operational hours.

II. METHODS

A. The studied LFR system

This work uses an LFR installed according to a North-South orientation and made up of ten rows; five rows on each side of the receiver. Each row contains three flat reflecting mirrors of 0.5 m in width and 3 m in length. The receiver is an evacuated tube of 0.125 m in radius installed 2 m above the reflecting mirrors. A semi-cylindrical secondary concentrator of 0.25 m in radius is mounted overhead the evacuated tube. The studied LFR uses non-equidistant spacing between adjacent rows modeled utilizing the validated method the authors developed and presented during the International Renewable and Sustainable Energy Conference (IRSEC) of 2014 held in Ouarzazat, Morocco [1]. This method relies on a specific Design Profile Angle (DPA) to calculate the appropriate spacing between two adjacent rows of reflecting mirrors to avoid mutual shading between them. This wok uses a DPA varying from 10° to 50°.

B. The optical efficiency of the LFR system

The optical efficiency, $\eta_o(\theta)$, of a CSP technology is defined as the ratio of the radiation that reaches the receiver to the radiation that fall on the solar field [2]. In the case of an LFR system, $\eta_o(\theta)$ is generally written as a product of two parameters as presented in equation 1. In this equation, $\eta_o(\theta = 0^\circ)$ stands for the optical efficiency of the solar field at normal incidence angle. It is the reference optical efficiency that is multiplied by the Incidence Angle Modifier, IAM, to get the actual optical efficiency of the system at a given time of the day. The IAM is a correction function introduced to the reference optical efficiency to account for the change in the solar field optics due to the change of the sun's position in the sky [3], [4]. The IAM is bi-dimensional for LFR systems and it is generally factorized using the method of McIntire as in equation 2 [5]. In this equation,

IAM_T stands for the transversal incidence angle modifier representing the variation of the solar field optics according to the variation of the transversal incidence angle θ_t and it accounts for shading, blocking and cosine effect [6], [7]. IAM_L stands for the longitudinal incidence angle modifier representing the change in the solar field optics according to the variation of the longitudinal incidence angle θ_l and it accounts for end loss and cosine effect [7], [8]. According to their definitions, IAM_T and IAM_L are calculated using equations 3.

$$\eta_o(\theta) = IAM(\theta) * \eta_o(\theta = 0^\circ) \quad (1)$$

$$IAM(\theta) = IAM_T(\theta_t) * IAM_L(\theta_l) \quad (2)$$

$$IAM_T(\theta_t) = \frac{\eta_o(\theta=\theta_t)}{\eta_o(\theta=0^\circ)} \quad \text{and} \quad IAM_L(\theta_l) = \frac{\eta_o(\theta=\theta_l)}{\eta_o(\theta=0^\circ)} \quad (3)$$

In all available studies $\eta_o(\theta = 0^\circ)$, IAM, IAM_T, and IAM_L are calculated using ray tracing [9]–[19]. Some authors used software specialized in the raytracing field like Raytrace3D [20], Soltrace [21], Tonatiuh [8], and TracePro [22]–[24]. Instead, others chose to develop their own codes relying on the Monte Carlo Raytracing method and usually implemented in Matlab [9], [11], [14].

In this work, the authors used the Monte Carlo Raytracing software TracePro to simulate the optical efficiency of the studied LFRs. In fact, five different LFRs were built in the 3D environment of the software; each system is modeled according to a specific DPA. One million rays were applied by total solar field area. The position of the rays' source was varied from 5° to 90° by a 5° step in the longitudinal and in the transversal planes separately. Data concerning the reflected rays that reach the outer surface of the absorber tube were collected and used to calculate the values and variations of IAM_T and IAM_L. Obtained results were then implemented in a code to evaluate the hourly, daily and annual variation of IAM and $\eta_o(\theta)$.

C. Application to the case study

To evaluate the amount of heat transferred to the outer surface of the absorber tube at a given location, the following equation is used [25]–[27]:

$$Q_{in} = DNI * \eta_o(\theta) * A_m \quad (4)$$

Where:

- Q_{in} , given in W, is the heat transferred to the outer surface of the absorber tube;
- DNI, given in W/m², is the direct normal irradiance;
- $\eta_o(\theta)$, is the overall optical efficiency of the system;
- A_m , given in m², is the total solar field area.

A code allowing the estimation of Q_{in} on an hourly, daily, monthly and annual basis was written and used to compare the performances of the studied LFR system at five different locations. These locations are well-known cities spread over three different continents and five different countries as it is shown in table 1. When choosing the cities to work on, we tried our best to have a difference in latitude of 10° between two consecutive cities.

TABLE I
DETAILS OF THE CITIES CHOSE FOR THE CASE STUDY

Continent	Country	City	Latitude (φ)	Longitude	Elevation (m)
Africa	Ghana	Accra	5.6°	-0.17°	69
Africa	Ethiopia	Addis Ababa	8.98°	38.8°	2355
Asia	Kingdom of Saudi Arabia	Riyadh	24.7°	46.8°	612
Africa	Egypt	Cairo	30.13°	31.4°	74
Europe	Spain	Madrid	40.45°	-3.55°	582

Hourly DNI data of these five cities were derived from the website www.energyplus.net, which is managed by the National Renewable Energy Laboratory (NREL) [28]. Since available data are provided on an hourly basis, equations 5, 6, and 7 were used to evaluate daily, monthly, and annual mean DNI. Figure 1 presents the available energy expressed in terms of available monthly mean DNI at these five different locations.

These five cities will be compared using the heat transferred to the outer surface of the absorber tube per month and per year, and operational hours per year.

$$\text{daily DNI} = \frac{1}{t_{ss} - t_{sr}} \int_{t_{st}=t_{sr}}^{t_{st}=t_{ss}} \text{hourly DNI } d(st) \quad (5)$$

$$\text{monthly DNI} = \frac{1}{\text{number of days per month}} \int \text{daily DNI } d(\text{doy}) \quad (6)$$

$$\text{annual DNI} = \frac{1}{365-1} \int_{\text{doy}=1}^{\text{doy}=365} \text{daily DNI } d(\text{doy}) \quad (7)$$

Where st is solar time, t_{sr} is sunrise time, t_{ss} is sunset time, and doy is day of the year.

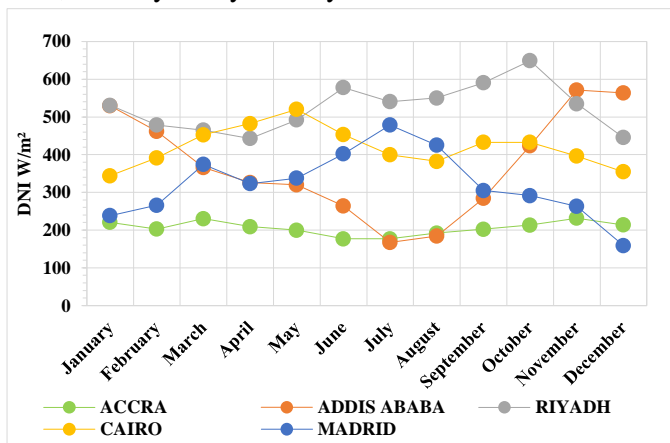


Figure 1: Available monthly mean DNI at the studied locations

III. RESULTS AND DISCUSSION

A. Analysis of the reference optical efficiency

In this subsection we analyze the impact of the DPA, the solar field width, and the solar field length on the $\eta_o(\theta=0^\circ)$ of the studied LFR. Results obtained are presented in figures 2 and 3. The first one presents the variation of $\eta_o(\theta=0^\circ)$ and of the total LFR area according to DPA while the second one presents the variation of $\eta_o(\theta=0^\circ)$ according to the variation of the width of the LFR solar field for DPA=40°. The width of the studied LFR was modified by adding more rows of reflecting mirrors to the solar field.

It is observed that increasing the DPA from 10° to 50° led to an increase in $\eta_o(\theta=0^\circ)$ from 11.09% to 23.56% while it led to a decrease in the total LFR area from 96.82 m² to 54.05 m². At low DPAs, the LFR occupied

a large area with a weak $\eta_o(\theta=0^\circ)$. On the opposite, high DPAs led to smaller occupied area by the LFR with high $\eta_o(\theta=0^\circ)$.

In fact, smaller spacing is required between adjacent rows to avoid mutual shading between reflecting mirrors the case of high DPAs. This results in a smaller occupied land by the solar field and less incoming sunrays being lost in the unused spacing between rows leading to better $\eta_o(\theta=0^\circ)$. On the other hand, varying the length of the LFR did not affect the $\eta_o(\theta=0^\circ)$, thus we only present results related to varying the solar field width. It is clear from figure 3 that a maximum $\eta_o(\theta=0^\circ)$ of 22.33% was reached by the solar field made of 12 rows. This is because adding more rows to the solar field will make it intercept more incoming sunrays and therefore have a better $\eta_o(\theta=0^\circ)$. Yet, exceeding a given number of rows, losses due to shading and blocking will become much important leading to a decrease in $\eta_o(\theta=0^\circ)$. This behavior reveals that an optimum solar field width exists that developers should seek for when sizing their own LFRs to maximize $\eta_o(\theta=0^\circ)$.

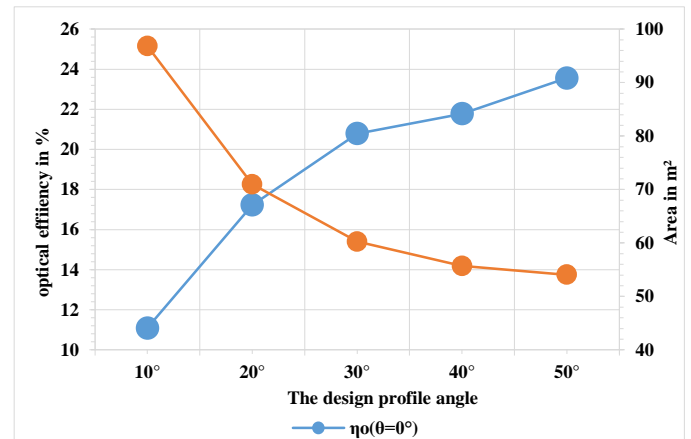


Figure 2: Variation of the reference optical efficiency and the total LFR solar field area according to different design profile angles

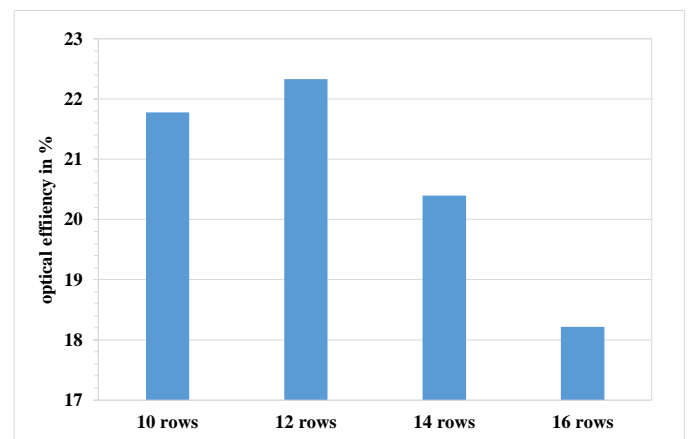
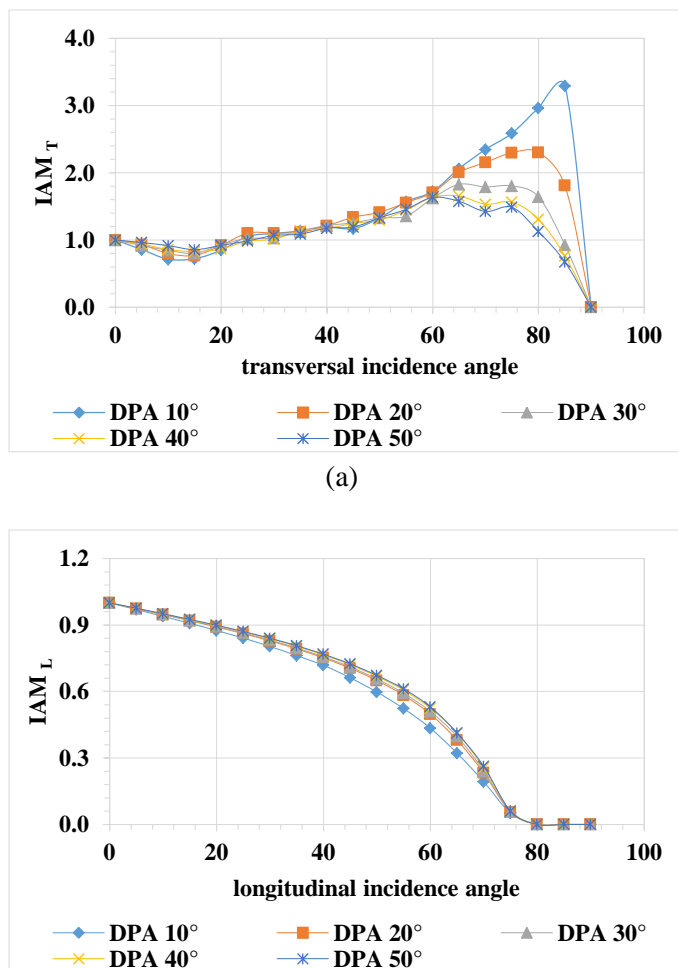


Figure 3: Variation of the reference optical efficiency according to the total solar field width

B. Analysis of the Incident Angle Modifier

This subsection is meant to study the behavior of the IAM. We discuss the impact of the DPA, the solar field width, the solar field length, day of the year, and time of the day on the IAM itself as well as on its two components IAM_T and IAM_L. Results obtained are presented in figures 4-6.

Figure 4 illustrates the change that occurs to IAM_T and IAM_L when changing θ_t and θ_l according to different DPAs. Changing the DPA did not affect the IAM_L unlike IAM_T that decreased with the increase of DPA especially at $\theta_t > 60^\circ$. Actually, changing the DPA only affects the spacing between adjacent rows of reflecting mirrors, thus the IAM_L is not concerned by it. On the opposite, increasing the DPA makes the solar field more tight resulting in higher shading and blocking losses. And given that the main optical effects incorporated in IAM_T are shading and blocking, this will naturally lead to a decrease in IAM_T.



(b)

Figure 4: Variation of the transversal incident angle modifier according to θ_t (a) and the variation of the longitudinal incident angle modifier according θ_l (b)

Figure 5 presents the variation of IAM_T according to θ_t for different solar field widths (left) and the variation of IAM_L according to θ_l for different solar field lengths (right). The IAM_T did not change much when the total width of the solar field changed especially for $\theta_t < 65^\circ$. On the opposite, changing the total length of the solar field had a significant impact on the IAM_L since longer solar fields recorded better IAM_L. Moreover, the IAM_L of the longest solar field reached zero 5° after the shorter ones did. Indeed, as it was reported in the introduction section, longer solar fields suffer from less end loss effect, which is the main optical effect present within the longitudinal plane. Consequently, better IAM_L are achieved in the case of longer solar fields.

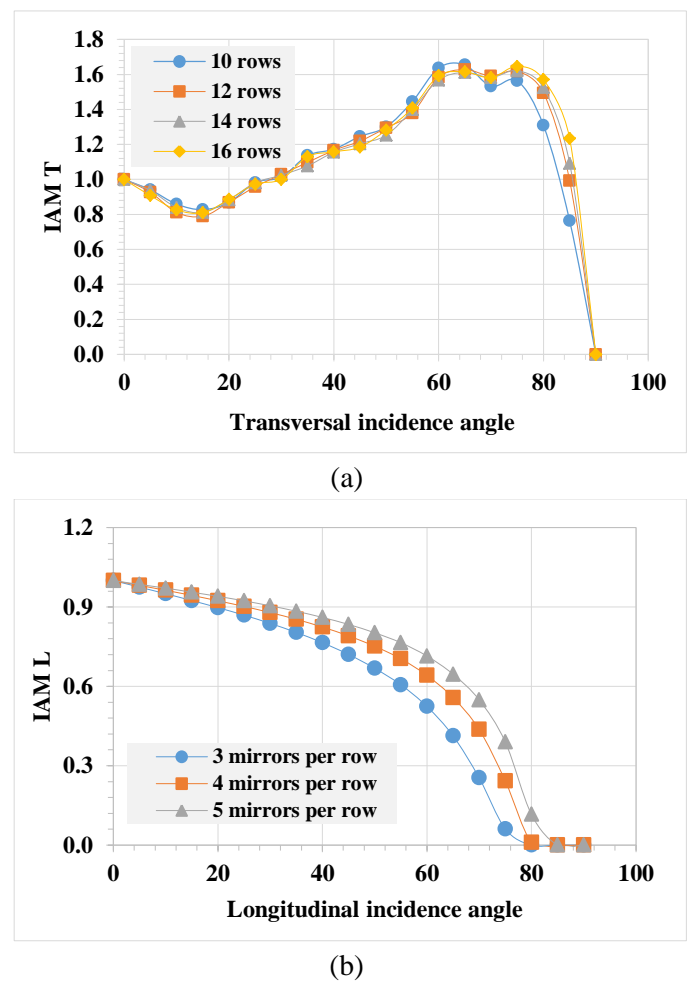


Figure 5: Variation of the IAM_T according to θ_t for different solar field widths (a) and variation of the IAM_L according to θ_l for different solar field lengths (b)

Figure 6 shows the hourly variation of IAM_T , IAM_L , and IAM during four typical days characterizing each season of the year, which are the two equinoxes (21st March and 21st September) and the two solstices (21st Jun and 21st December). Displayed results are those obtained for $\phi=30^\circ$ and $DPA=50^\circ$. It is observed that the variation in seasons had a significant impact on IAM_L unlike IAM_T that remained the same. Actually, hourly IAM_L recorded two maximums (equal 1.5) during the summer solstice; one in the early morning and the other late in the afternoon while it only had one maximum during the winter solstice not exceeding 0.75. In what concerns the IAM , its behavior completely changed from a season to another derived by the heavy change in its longitudinal component. In fact, the IAM presented two maximums a day during the summer solstice and the two equinoxes with higher values reached in the summer. Instead, it reached very low values during the winter solstice with a nearly constant behavior during the whole day. The seasonal variation of the IAM_L and IAM_T is highly influenced by the seasonal variation of the optical effects they incorporate. Indeed, shading and blocking losses, which are the main effects influencing IAM_T , do not vary much along the year as was reported by Vashi Sharma in [15]. Consequently, IAM_T is not affected by the change in seasons. By contrast, the heavy change in IAM_L reflects the strong relationship it has with end loss effect that varies significantly according to season as reported in . Moreover, the hourly variation of end loss efficiency reported by the authors in a previously published paper is similar in its general trend to the hourly variation of IAM_L reported herein [22].

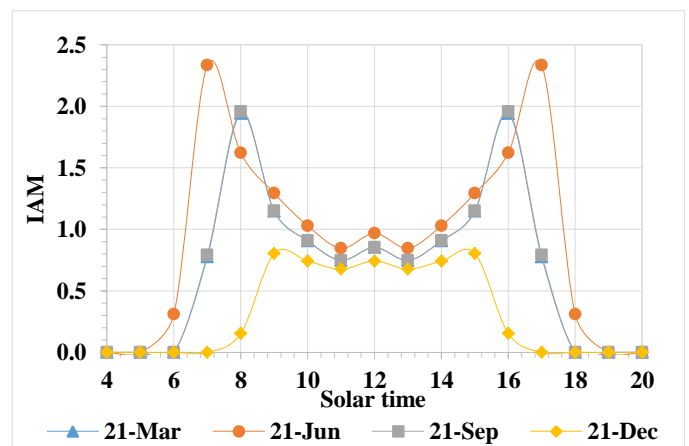
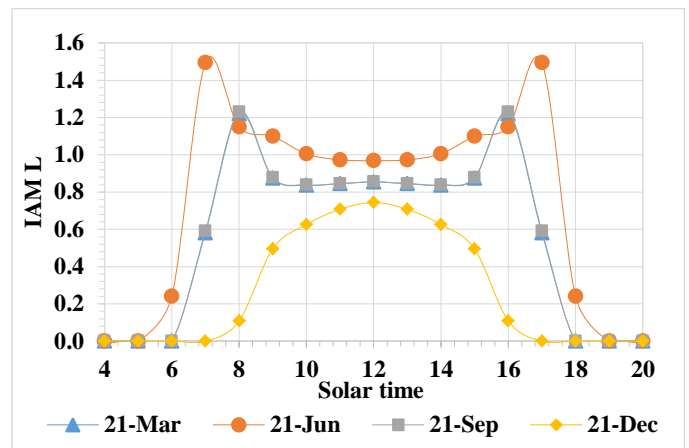
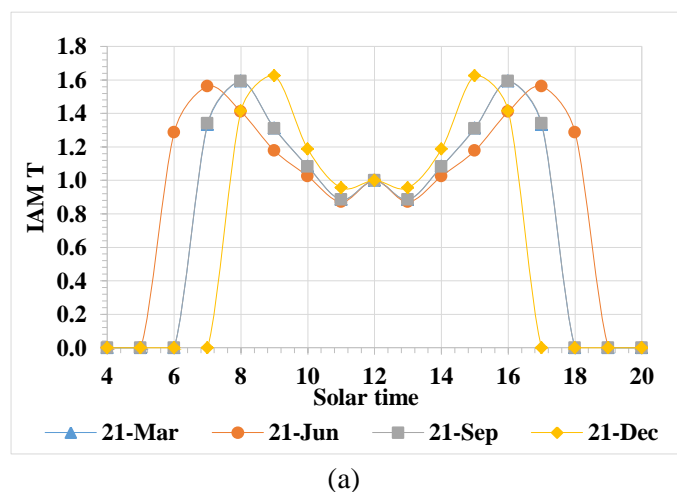


Figure 6: Hourly variation of IAM_T (a), IAM_L (b), and IAM (c) during the two equinoxes and the two solstices of the year

C. Analysis of the optical efficiency

This subsection is dedicated to the parametric evaluation of the overall optical efficiency of the studied LFR on an hourly, daily and annual basis. Two parameters are considered: the DPA and the location's latitude where the LFR is installed. Obtained results are depicted in figures 7-10.

Figure 7 illustrates the hourly variation of the optical efficiency of the LFR considering different DPAs at $\phi = 30^\circ$. It is clear that better results was obtained using high DPAs. The same trend was recorded for all DPAs; the optical efficiency had two maximums a day one early in the morning and the other late in the afternoon with some fluctuations around midday. This general trend is clearly dictated by the trend of the IAM . However, obtained results show the importance of $\eta_o(\theta=0^\circ)$ in determining the overall optical efficiency of

a given LFR. In fact, low DPAs have the best IAMs but recorded the worst optical efficiencies due to their low $\eta_o(\theta=0^\circ)$. In what concerns the fluctuations observed around midday, they are the consequence of the secondary concentrator that starts to cast its shadow on the reflecting mirrors at this time of the day. When taking shading of the secondary concentrator into consideration, three cases are to discuss. The first case is when only one mirror finds itself or part of it under shading of the secondary concentrator. The second case is when shading of the secondary concentrator falls entirely on the spacing between rows, thus it is like if it does not occur at all. The last case is when shading of the secondary concentrator touches parts of two consecutive mirrors.

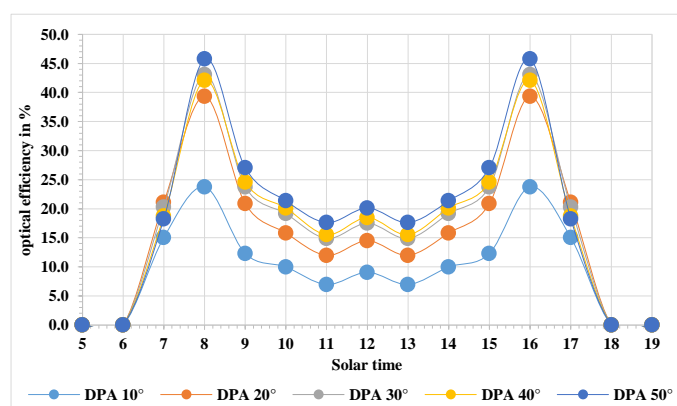


Figure 7: Hourly variation of the optical efficiency for different DPAs

Figure 8 presents the variation of the optical efficiency of the studied LFR on a daily basis considering different ϕ for DPA=50°. As shown, two maximums are recorded both around the two equinoxes with a decrease in the optical efficiency during the summer. This behavior was common to all DPAs with better results reached by the highest ones. Meanwhile, this behavior changed at high ϕ for which the two maximums were closer to the summer solstice than to the two equinoxes. In addition, the decrease in the optical efficiency during the summer nearly disappeared at high ϕ . The same behavior was reported in some recent published papers [5], [19].

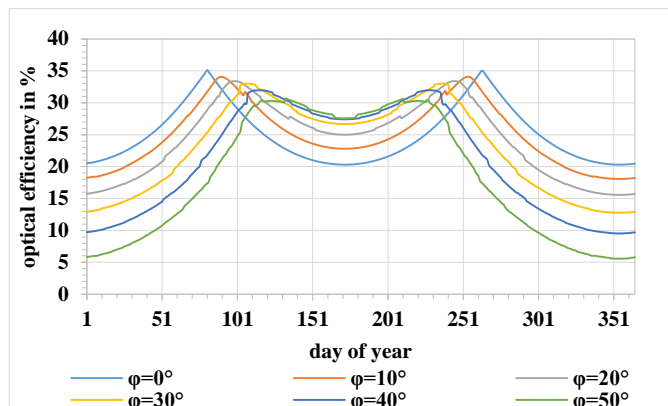


Figure 8: Daily variation of the LFR solar field optical efficiency for DPA=50° according to different latitudes

In figure 9, the variation of the annual optical efficiency is plotted against the variation of latitude considering different DPAs. One may observe that the highest DPAs led to the best results especially at the equator where all maximums had been recorded. In fact, the overall best annual optical efficiency equals 25% was reached by DPA=50° at the equator. Moreover, it is observed that the annual optical efficiency did not vary significantly until $\phi=20^\circ$. Exceeding this latitude, annual optical efficiency started to decrease rapidly. These results show that the best locations to operate an LFR is somewhere near the equator using a high DPA in the modeling process of the solar field. This comes in accordance with what was concluded by Abbas and Martinez-Val in a recent published paper [44]. Meanwhile, it should be pointed that high DPAs also lead to bigger occupied land that should be taken into consideration especially in places where land is expansive or limited.

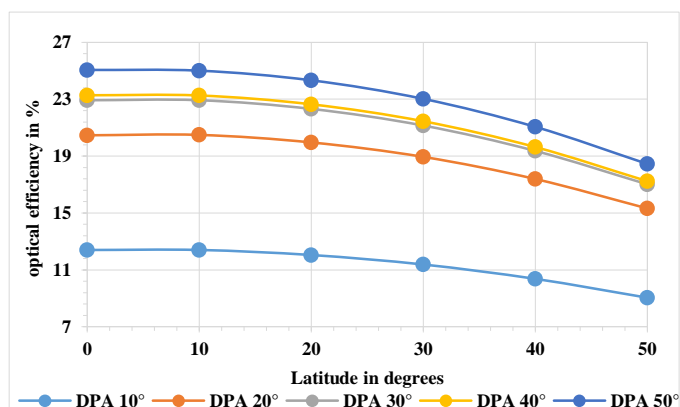


Figure 9: Variation of annual optical efficiency for different DPAs according to latitude

D. The case study

In this subsection, another factor is introduced in our study of the LFR system, which is the available heat at the absorber tube. For this purpose, five different cities at five different locations of the world were considered. Obtained results are presented in figures 10 and 11.

Figure 10 shows the variation of monthly mean heat transferred to the receiver expressed in W/month for the five studied cities while figure 11 shows the variation of annual mean heat transferred to the receiver and annual available heat both expressed in W/year alongside with operational hours. The first thing noticed is the heavy variability of transferred heat from month to month especially at high ϕ . This fact makes the sizing of the power-block a tricky task at such locations. For annual performances, it showed clearly that Riyadh recorded the best results with an annual mean transferred heat of 7030 W/year, and was operational during 3636 hours/year. Addis Ababa and Cairo had comparable performances in what concerns transferred heat per year even they had different operational hours per year. One interesting location was Accra that had operational hours longest than Riyadh and Cairo, but it recorded the overall worst results in terms of annual mean heat transferred to the receiver. These results show that the optical analysis of the LFR system is not sufficient to predict its performances. The available energy resources (DNI) at a given location play an important role in the determination of how much the LFR system will make use of its high optical efficiency. In fact, while the optical analysis predicted that locations near the equator ($\phi < 20^\circ$) will achieve the best results, the case study shows that the best performances are obtained in locations with latitudes over 20° .

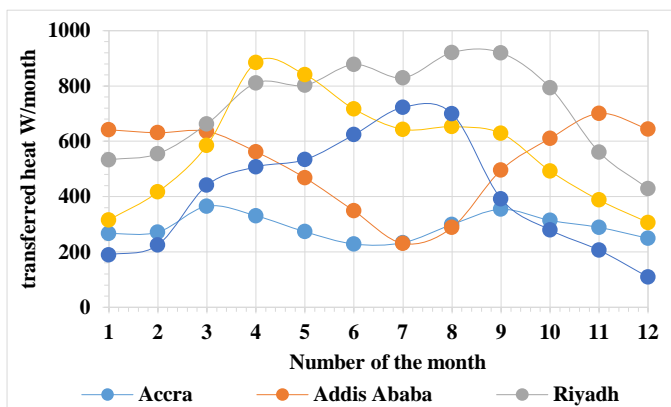


Figure 10: Variation of monthly heat transferred to the receiver expressed in W/month

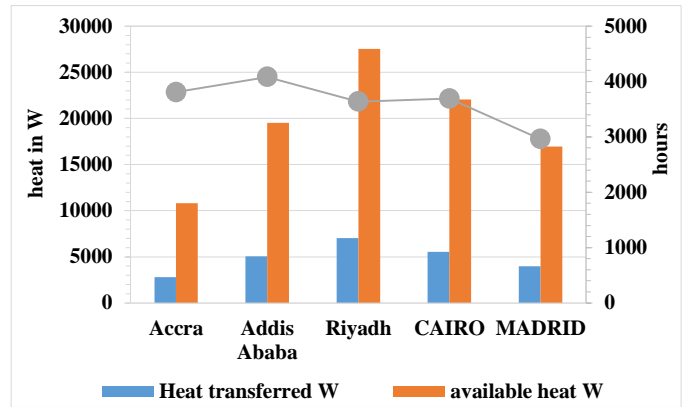


Figure 11: Variation of annual available heat and annual heat transferred expressed in W/year alongside with operational hours

IV. CONCLUSION

This study contributed to enhance our understanding of the optical issue of the LFR system through a parametric analysis that uses a Monte Carlo Ray Tracing tool. This analysis focused on $\eta_o(\theta=0^\circ)$ and IAM with its two components IAM_L and IAM_T . Obtained results showed that the optical efficiency at normal incidence, $\eta_o(\theta=0^\circ)$, increased when the DPA increased. In fact, the highest $\eta_o(\theta=0^\circ)$, equals 23.56%, was recorded by the highest DPA, equals 50° . However, $\eta_o(\theta=0^\circ)$ decreased when the solar field incorporated too many rows of reflecting mirrors. The way $\eta_o(\theta=0^\circ)$ varied when adding more rows to the solar field showed that there is an optimum width developers should seek for when modeling their LFR systems. On the other hand, IAM showed a season related behavior with better results recorded around the two equinoxes of the year. In addition, the IAM reached higher values at low ϕ . The overall optical efficiency revealed that the best locations to operate an LFR was around the equator while the best DPA to use in the modeling process of the solar field was the highest one. The case study showed that the available energy resources are of great importance in the prediction of the LFR overall performances regardless of the optical efficiency. In addition, results showed the great variability of monthly mean heat transferred especially at high ϕ . In terms of annual results, low ϕ had the worst results while cities at higher ϕ such Riyadh was found to be the best locations to operate an LFR.

V. REFERENCES

- [1] D. Nakar and D. Feuermann, "Surface roughness impact on the heat loss of solar vacuum heat collector elements (HCE)," *Renew. Energy*, vol. 96, pp. 148–156, Oct. 2016.
- [2] M. Romero and A. Steinfeld, "Concentrating solar thermal power and thermochemical fuels," *Energy Environ. Sci.*, vol. 5, no. 11, p. 9234, 2012.
- [3] M. Romero and J. González-Aguilar, "Solar thermal CSP technology: Solar thermal CSP technology," *Wiley Interdiscip. Rev. Energy Environ.*, vol. 3, no. 1, pp. 42–59, Jan. 2014.
- [4] J. Petrasch and J. Klausner, "Integrated solar thermochemical cycles for energy storage and fuel production: Integrated solar thermochemical cycles," *Wiley Interdiscip. Rev. Energy Environ.*, vol. 1, no. 3, pp. 347–361, Nov. 2012.
- [5] Y. Qiu, Y.-L. He, Z.-D. Cheng, and K. Wang, "Study on optical and thermal performance of a linear Fresnel solar reflector using molten salt as HTF with MCRT and FVM methods," *Appl. Energy*, vol. 146, pp. 162–173, May 2015.
- [6] A. Heimsath, F. Cuevas, A. Hofer, P. Nitz, and W. J. Platzer, "Linear Fresnel Collector Receiver: Heat Loss and Temperatures," *Energy Procedia*, vol. 49, pp. 386–397, 2014.
- [7] M. K. Gupta, S. C. Kaushik, K. R. Ranjan, N. L. Panwar, V. S. Reddy, and S. K. Tyagi, "Thermodynamic performance evaluation of solar and other thermal power generation systems: A review," *Renew. Sustain. Energy Rev.*, vol. 50, pp. 567–582, Oct. 2015.
- [8] S. Benyakhlef et al., "Impact of heliostat curvature on optical performance of Linear Fresnel solar concentrators," *Renew. Energy*, vol. 89, pp. 463–474, Apr. 2016.
- [9] R. Abbas and J. M. Martínez-Val, "Analytic optical design of linear Fresnel collectors with variable widths and shifts of mirrors," *Renew. Energy*, vol. 75, pp. 81–92, Mar. 2015.
- [10] V. Sharma, S. Khanna, J. K. Nayak, and S. B. Kedare, "Effects of shading and blocking in compact linear fresnel reflector field," *Energy*, vol. 94, pp. 633–653, Jan. 2016.
- [11] J. D. Hertel, V. Martinez-Moll, and R. Pujol-Nadal, "Estimation of the influence of different incidence angle modifier models on the biaxial factorization approach," *Energy Convers. Manag.*, vol. 106, pp. 249–259, Dec. 2015.
- [12] G. Zhu, "Development of an analytical optical method for linear Fresnel collectors," *Sol. Energy*, vol. 94, pp. 240–252, Aug. 2013.
- [13] M. J. Montes, C. Rubbia, R. Abbas, and J. M. Martínez-Val, "A comparative analysis of configurations of linear Fresnel collectors for concentrating solar power," *Energy*, vol. 73, pp. 192–203, Aug. 2014.
- [14] P. Boito and R. Grena, "Optimization of the geometry of Fresnel linear collectors," *Sol. Energy*, vol. 135, pp. 479–486, Oct. 2016.
- [15] V. Sharma, "Hourly and Monthly Variation in Shading and Blocking of Aperture Area in a Linear Fresnel Reflector Field," *Energy Procedia*, vol. 48, pp. 233–241, 2014.
- [16] V. Sharma, J. K. Nayak, and S. B. Kedare, "Effects of shading and blocking in linear Fresnel reflector field," *Sol. Energy*, vol. 113, pp. 114–138, Mar. 2015.
- [17] H. H. Sait, J. M. Martinez-Val, R. Abbas, and J. Munoz-Anton, "Fresnel-based modular solar fields for performance/cost optimization in solar thermal power plants: A comparison with parabolic trough collectors," *Appl. Energy*, vol. 141, pp. 175–189, Mar. 2015.
- [18] A. Barbón, N. Barbón, L. Bayón, and J. A. Otero, "Theoretical elements for the design of a small scale Linear Fresnel Reflector: Frontal and lateral views," *Sol. Energy*, vol. 132, pp. 188–202, Jul. 2016.
- [19] Y. Qiu, Y.-L. He, M. Wu, and Z.-J. Zheng, "A comprehensive model for optical and thermal characterization of a linear Fresnel solar reflector with a trapezoidal cavity receiver," *Renew. Energy*, vol. 97, pp. 129–144, Nov. 2016.
- [20] A. Heimsath, G. Bern, D. van Rooyen, and P. Nitz, "Quantifying Optical Loss Factors of Small Linear Concentrating Collectors for Process Heat Application," *Energy Procedia*, vol. 48, pp. 77–86, 2014.
- [21] Y. Elmaanaoui and D. Saifaoui, "Shading efficiency calculation for Linear Fresnel reflector," in *Renewable and Sustainable Energy Conference (IRSEC), 2014 International*, 2014, pp. 100–103.
- [22] Y. Elmaanaoui and D. Saifaoui, "Parametric analysis of end loss efficiency in linear Fresnel reflector," in *2014 International Renewable and Sustainable Energy Conference (IRSEC), 2014*, pp. 104–107.

- [23] J. D. Nixon and P. A. Davies, "Cost-exergy optimisation of linear Fresnel reflectors," *Sol. Energy*, vol. 86, no. 1, pp. 147–156, Jan. 2012.
- [24] D. R. Mills and G. L. Morrison, "Compact linear Fresnel reflector solar thermal powerplants," *Sol. Energy*, vol. 68, no. 3, pp. 263–283, 2000.
- [25] J. Chaves and M. Collares-Pereira, "Etendue-matched two-stage concentrators with multiple receivers," *Sol. Energy*, vol. 84, no. 2, pp. 196–207, Feb. 2010.
- [26] J. D. Nixon and P. A. Davies, "Construction and experimental study of an elevation linear Fresnel reflector," *J. Sol. Energy Eng.*, vol. 138, no. 3, p. 31001, 2016.
- [27] S. A. Kalogirou, "Solar thermal collectors and applications," *Prog. Energy Combust. Sci.*, vol. 30, no. 3, pp. 231–295, Jan. 2004.
- [28] F. Yang et al., "Acceptance Testing Procedure for Linear Fresnel Reflector Solar Systems in Utility-Scale Solar Thermal Power Plants," *Energy Procedia*, vol. 69, pp. 1479–1487, May 2015.
- [29] W. R. McIntire, "Factored approximations for biaxial incident angle modifiers," *Sol. Energy*, vol. 29, no. 4, pp. 315–322, 1982.
- [30] P. Horta and T. Osório, "Optical Characterization Parameters for Line-focusing Solar Concentrators: Measurement Procedures and Extended Simulation Results," *Energy Procedia*, vol. 49, pp. 98–108, 2014.
- [31] R. Abbas, J. Muñoz-Antón, M. Valdés, and J. M. Martínez-Val, "High concentration linear Fresnel reflectors," *Energy Convers. Manag.*, vol. 72, pp. 60–68, Aug. 2013.
- [32] R. Abbas, M. J. Montes, M. Piera, and J. M. Martínez-Val, "Solar radiation concentration features in Linear Fresnel Reflector arrays," *Energy Convers. Manag.*, vol. 54, no. 1, pp. 133–144, Feb. 2012.
- [33] R. Abbas et al., "A Quest to the Cheapest Method for Electricity Generation in Concentrating Solar Power Plants," *Energy Procedia*, vol. 75, pp. 514–520, Aug. 2015.
- [34] G. Zhu, T. Wendelin, M. J. Wagner, and C. Kutscher, "History, current state, and future of linear Fresnel concentrating solar collectors," *Sol. Energy*, vol. 103, pp. 639–652, May 2014.
- [35] H. L. Zhang, J. Baeyens, J. Degève, and G. Cacères, "Concentrated solar power plants: Review and design methodology," *Renew. Sustain. Energy Rev.*, vol. 22, pp. 466–481, Jun. 2013.